Advanced Ceramics Progress: Vol. 7, No. 4, (Autumn 2021) 36-51

Materials and Energy Research Center
MERC

Contents lists available at ACERP

Advanced Ceramics Progress

Journal Homepage: www.acerp.ir

Original Research Article

Experimental and Numerical Study of the Thermo-Mechanical Behavior of Plasma-Sprayed Gadolinium and Yitria Zirconate-Based Thermal Barrier Coatings

N. Nayebpashaee [a,*], E. Etemadi [b], B. Mohammad Sadeghi [c], S. H. Seyedein [d]

[a] *Assistant Professor, Department of Metallurgy and Mechanical Engineering, Technology and Engineering Research Center, Standard Research Institute (SRI), Karaj, Alborz, Iran*

[b] *PhD Candidate, Faculty of Materials Science and Engineering, Malek Ashtar University, Tehran, Tehran, Iran*

[c] *Assistant Professor, School of Metallurgy and Materials Engineering, Iran University of Science and Technology, Tehran, Tehran, Iran*

[d] *Professor, School of Metallurgy and Materials Engineering, Iran University of Science and Technology, Tehran, Tehran, Iran*

* Corresponding Author Email: n.nayebpashaee@standard.ac.ir (N. Nayebpashaee) URL: https://www.acerp.ir/article_144395.html

ARTICLE INFO

Article History:

Received 01 January 2022
Received in revised form 02 February 2022
Accepted 06 February 2022

Keywords:

Functionally Graded Thermal Barrier Coating (FGTBC)
Thermal Shock
Residual Stress
Nano-Indentation
Finite Element Method

ABSTRACT

The current study aims to analyze the thermal and residual stress distributions in both duplex and functionally-graded thermal barrier coatings (TBCs) of yttria-stabilized zirconia (YSZ) and gadolinium zirconate (GZ) during a realistic heating regime. To this end, finite element model was employed to model the effects of thermal loading on the thermomechanical response and stress distribution. In addition, three different YSZ-based TBC systems, one duplex, and two FG-TBCs were fabricated using the APS method. The coatings were characterized based on SEM/EDS, map analysis, and XRD. The residual stress, elastic modulus, microhardness, and fracture toughness of the coatings were determined using nanoindentation method. The obtained results revealed that the microstructure, porosity, and chemical composition changed gradually due to the functionally-graded coating. Examination of the surface of the samples after the application of thermal shock showed that the separation of the layers occurred more frequently in the cases of two-layer coatings than in the graded ones. The contours of the heat flux and nodal temperatures confirmed that most of the damaging thermal residual stresses were concentrated in the ceramic top coat, thus resulting in less damage and life-shortening of the substrate. The magnitude of the residual stress in the FG-TBC was lower than that in the duplex TBC, and the stress distribution was more uniform, hence improvement in the performance and extention of the life of the thermal barrier system. According to the findings, the YSZ-based TBC outperformed the gadolinium zirconate-based TBC in terms of thermal shock resistance and residual stress.

https://doi.org/10.30501/ACP.2022.322563.1078

1. INTRODUCTION

Tolerance of higher temperatures in different parts of internal combustion engines has always been an important concern in aerospace and turbine industries. Thermal Barrier Coatings (TBCs) are regarded as important elements in the durability of hot section components. They function as the insulating components such as turbine blades, combustor cans, ducting and nozzle guide vanes operating at elevated temperature. In

Please cite this article as: Nayebpashaee, N., Etemadi, E., Mohammad Sadeghi, B., Seyedein, S. H., "Experimental and Numerical Study of the Thermo-Mechanical Behavior of Plasma-Sprayed Gadolinium and Yitria Zirconate-Based Thermal Barrier Coatings", ***Advanced Ceramics Progress***, Vol. 7, No. 4, (2021), 36-51. https://doi.org/10.30501/ACP.2022.322563.1078

addition, they make an increase in the operating temperature of gas turbines possible [1-5].

The typical TBC is composed of three layers namely Bond Coat (BC), Top Coat (TC), and Thermally Grown Oxide (TGO). The BC is made of MCrAlY (with M=Ni and/or Co), and the TC often consists of a thermal barrier layer based on Yttria-Stabilized Zirconia (YSZ) [1-3]. At high temperatures, oxygen is transferred from the TC to the BC through micro cracks and interconnected pinholes within the TC. During the operation, aluminum in the BC diffuses and reacts with oxygen from the combustion gases. As a result, an oxidized scale of alumina (Al_2O_3) is formed on the BC called the TGO layer which is primarily related to the oxidation of the BC. The major disadvantages of YSZ are the limited operational temperature resulting from the phase transformation, sintering induced volume shrinkage, and low corrosion resistance. To overcome these drawbacks, the necessity of searching for new alternative materials is highlighted more than ever [1,6-8]. Zirconate-based TBCs are expected to be appropriate candidates for future applications in high-temperature components due to their low thermal conductivity, high stability, and high sintering resistance at high temperatures [1,8]. Gadolinium Zirconate ($Gd_2Zr_2O_7$ or GZ) is another candidate material that is a new and promising alternative ceramic coating material to YSZ that enjoys several major advantages such as higher thermal stability at elevated temperatures and lower thermal conductivity (1.3 W/mK^{-1} at 1100 °C), and better hot corrosion resistance than those of YSZ (1.8 W/mK^{-1} at 1100 °C), thus potentially allowing better thermal insulation [9,10].

Some problems may arise in the case of plasma-sprayed TBC such as spallation caused by the TGOs with different thickness values and morphologies as well as cracking in long-term services due to their poor bond strength and high residual stresses. Functionally Graded Thermal Barrier Coatings (FG-TBCs) with a gradual compositional variation from the TCto the BC were proposed to overcome these limitations. The microstructural grading of FG-TBCs could help reduce the mismatch in thermomechanical properties. In addition, using FG-TBCs may improve other properties such as adhesion, corrosion, and oxidation [4,5,11].

Evaluating and measuring the residual stresses is of high importance in industry in determining the lifetime of the components. The measurement techniques for residual stress in the coatings can be divided into two groups of destructive and non-destructive methods. The non-destructive methods measure some parameters that are related to the stress. X-ray or neutron diffraction are referred to as the non-destructive methods, and the hole-drilling and layer removal method are regarded as the destructive ones. Nanoindentation is an indentation method for testing the hardness and other related mechanical properties of materials. It is also used to estimate the residual stress in thin films and coatings [12-15].

According to the literature, several experimental, analytical, and numerical studies have been conducted on the residual stress, crack evolution, failure mechanism, splatting impact, TGO and layer thickness, and thermal shock resistance of the TBCs [7,8,16-20]. For instance, Z. Valefi and M. Saremi [7] evaluated the effects of plasma spray parameters, atomizing gas, and substrate preheat temperature on the microstructure and phase composition of YSZ coatings produced through the SPPS process. According to their findings, upon increasing the power of plasma, using hydrogen as the precursor atomizing gas, and increasing the substrate preheat temperature, the amount of non-pyrolyzed precursor in the coatings would decrease [7]. S. M. Yunus et al. [17] compared the thermal resistance of a the plasma sprayed multilayer (GZ/YSZ) TBC with that of the single-layer YSZ coating and found that the single-layer YSZ system performed 12 % better than the multilayer TBC system at 1250 °C [17]. N. Nayebpashaee et al. [19] simulated the residual stress distribution and fracture mode of the TBCs based on the micromechanical approach FE with and without considering the presence of two-phase TGO. Their obtained results showed acceptable agreement between the simulated and experimental failure and crack growth modes. J. Song et al. [21] evaluated the effect of the non-uniform growth of the TGO on the stress evolution and interfacial crack initiation using the finite element method. They concluded that the non-uniform growth of the TGO would increase the magnitude of the residual stress in the TC layers, thus leading to early initiation of interfacial cracks [21].

The current study aimed to investigate the thermal and residual stress distribution in duplex TBC and functionally graded YSZ and GZ-TBCs during a realistic heating regime including heating, operating time, and final cooling. Despite the common applications of functionally graded strategies in surface engineering, very few studies have been conducted on the numerical aspects of functionally graded TBCs with novel zirconate (GZ) composition as the top ceramic layer TBCs in the literature. In addition, limited studies have focused on the thermal shock behavior of the TBC containing GZ as the TC so far.

2. MATERIALS AND METHODS

Yitria Zirconate-based TBC is usually applied in experimental studies. The used powders for bond and top coats were prepared according to the instructions given in Table 1. Prior to spraying, the starting powders were heat-treated at 100 °C for two hours to remove moisture. To obtain better substrate roughness and a clean surface, the Inconel (substrate) was blasted with silicon carbide particles with a mesh count of 25 in. at the optimum

pressure of four bars, followed by smooth grinding, degreasing, and acid pickling. Table 2 lists the plasma spray parameters used for TBC coating. X-Ray Diffraction (XRD) analysis was carried out to evaluate the materials formed on the top surface of the coating and characterize the coating surface after cooling the sprayed sample using a Siemens D 500 instrument. A thermal cycle was taken into account at the dwell time of 300 seconds and temperature of 1300 °C to perform the thermal shock. The samples were heated to the target temperature of 1300 °C in an electric furnace with air and then cooled to 25 °C using an air blast unit.

The thermal shocks with the oxidation time (cause of TGO formation) were repeated 45 times. Finally, to reveal the microstructure of the multiple shocked coatings in SEM studies, the samples were mounted, ground, and polished. The coating componenets were identified using OM, SEM/EDS, and mapping analysis.

TABLE 1. Specifications of powders used in plasma spraying

Layer	Composition	Powder	Morphology	Size (µm)
Top coat	ZrO_2-8 wt % Y_2O_3	Metco 204 –NS	Spherical	40-75
Bond coat	Ni-22Cr-10Al-1Y	AMDRY 962	Spherical	11-106

TABLE 2. Operating parameter of plasma spraying Inconel 738 used in this research

Parameter	Unit	YSZ (metco204Ns)	25 NiCrAlY + 75 YSZ	50 NiCrAlY + 50 YSZ	75 NiCrAlY + 25 YSZ	NiCrAlY (Amdry962)
Arc current intensity	A	500	500	500	450	450
Voltage	V	55	55	55	50	50
Carrier gas flow rate (Argon)	SCFH*	80	80	80	85	85
Carrier gas flow rate (Hydrogen)	SCFH	15	15	15	15	15
Powder carrier gas flow rate (Argon)	SCFH	30	30	30	30	30
Powder feed rate	lb/hr	25	20	20	15	15
Spray distance	cm	8	8	10	10	12
Injection diameter	mm	2	2	2	2	2
Cooling circulation system	-	water	water	water	water	water

*Standard Cubic Feet per Hour

2.1. Evaluation of Residual Stress by Nano Indentation Method

In this study, the residual stress was measured through nanoindentation method as well as indentation fracture technique. When using this technique to indent the surface of a brittle material with moderate force, it often produces a permanent impression with radially aligned cracks at the corner of the indent [12,22]. In order to calculate the residual stress, first, the mechanical properties of the coating such as Young's modulus, microhardness, and fracture toughness should be calculated. The calculation method is based on the methods presented in the previous study [23].

According to the load-depth curve, the hardness H and reduced modulus Er are defined by Equations 1 and 2 [23]:

$$H = \frac{P_{max}}{A_c} \quad (1)$$

$$E_r = \frac{\sqrt{\pi}}{2\beta}\frac{S}{\sqrt{A_c}} \quad (2)$$

where Pmax is the maximum load, A_c the contact area, $S = {}^{dP}/_{dh}$ the contact stiffness at initial unloading, and b a constant that depends on the geometry of the indenter. The reduced modulus E_r is defined through Equation (3) [23] as:

$$\frac{1}{E_r} = \frac{1-\vartheta_i^2}{E_i} + \frac{1-\vartheta_s^2}{E_s} \quad (3)$$

where E and E_i are the elastic modului of the specimen and indenter, respectively, and υ and υ_i are the Poisson's ratios of the specimen and indenter, respectively [23]. The Poisson's ratios of the TBC and diamond indenter are 0.2 and 0.07, respectively, and the valse of E_i for the diamond is 1141 GPa [24].

For Berkovich diamond indenter, we have $A_c = 24.49\ h_c^2 \approx 24.5\ h_c^2$ where h_c is the contact depth. Hence, Equation (1) will be as $H = \frac{P_{max}}{24.5\ h_c^2}$.

When a Vickers indenter is penetrated into the interface of two different materials, the fracture toughness for the

coating/BC interface is evaluated using Equation (4) [23]:

$$K_{IC} = \delta \left(\frac{E}{H}\right)^{1/2} \frac{P}{c^{3/2}} \quad (4)$$

where δ is the geometric factor and δ=0.015 for a Vickers indenter, and c= $(c_1+c_2+c_3)/3$ is the average length of three radial cracks with the lengths of c_1, c_2, and c_3 [23].

When applying the TBC containing stress and nanoindentation perpendicular to the cross-section of the TC layer in accordance with Figure 1, the fracture toughness is measured through Equation (5) [23]:

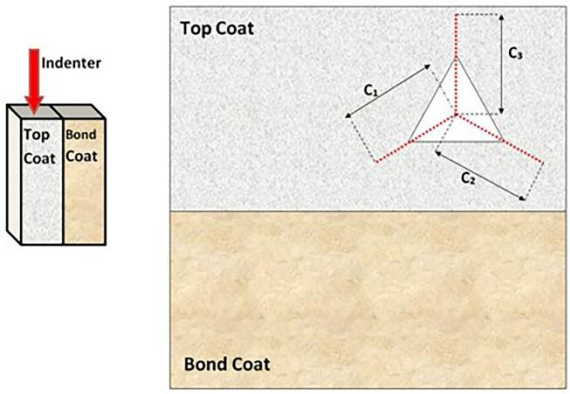

Figure 1. Schematics of Berkovich indentation perpendicular to the top coat of multiple-shocked coating

$$K_{IC} = \delta \left(\frac{E}{H}\right)_i^{1/2} \frac{P}{c^{3/2}} + \frac{2}{\sqrt{\pi}} \sigma c^{1/2} \quad (5)$$

Then, the ratio $P/c^{3/2}$ can be obtained as [23]:

$$\frac{P}{c^{3/2}} = \left(\frac{K_{IC}}{\chi_i}\right) + \left(-\frac{2\sigma}{\sqrt{\pi}\chi_i}\right) c^{1/2} \quad (6)$$

where $\chi_i = \delta\left(E/H\right)_i^{1/2}$. Equation (6) is regarded as a function of $c^{-1/2}$ where $\left(-\frac{2\sigma}{\sqrt{\pi}\chi_i}\right)$ and $\left(\frac{K_{IC}}{\chi_i}\right)$ denote the slope and intercept of Equation (6), respectively [23]. To obtain a better linear equation, a series of indentation tests should be carried out.

2.2. Performing Nano Indentation Test

A Triboscope system (Histron Inc. USA) was used to measure the stress in the nanoindentation method. A Berkovich diamond indenter was used for performing nanoindentation experiments. A device equipped with Atomic Force Microscopy (AFM) (NanoScope E, Digital Instruments, USA) was also used to examine the surface topography of the specimens. The values of the loading rate, pause time, and unloading rate were 5 mNs^{-1}, 5 s, and 5 mNs^{-1}, respectively. At room temperature, a series of forces ranging from 500 μN to 10,000 μN in increments of 1,000 μN were perpendicularly applied to the cross-section of the top layer of the multi-shocked TBC considering the YSZ. The length of the cracks was calculated using the image processing toolbox of the MATLAB software.

2.3. Finite Element Analysis

This section primarily aims to determine the temperature and stress distribution in the TBC. To this end, a simulation of TBC was performed using ABAQUS software. In addition, a two-dimensional finite element model was employed to numerically simulate the temperature distribution and consequent induced residual stress in the TBC. The schematic illustration of the studied area in the TBC system used in the hot section of the gas turbines is given in Figure 2.

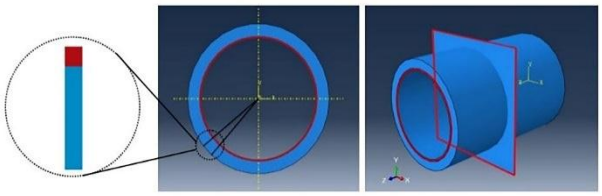

Figure 2. TBC calculation domain

As graphically shown in Figure 3, the duplex TBC system consists of both metallic and ceramic layers including an Inconel 738 substrate, a NiCoCrAlY sliding layer (BC), and GZ (YSZ) as a Top Layer (TC). The selected functionally graded TBC system used in this study is made of the following layers: an Inconel 738 substrate, a NiCoCrAlY bond (BC), 50 % BC + 50 % GZ (YSZ), and GZ (YSZ) as the top coat (Figure 3).

In order to obtain accurate results, appropriate thermal and mechanical boundary conditions should be considered. The thermal cycling applied at the highest level of the thermal barrier is shown in Figure 4. The heating cycle under study involves heating from 25 °C to 1300 °C in 30 seconds. In the second stage, it sustains temperature of 1300 °C for 200 seconds and in the third stage, it is cooled down from 1300 °C to 25 °C in 30 seconds.

In order to provide a suitable boundary condition for the bottom surface of the substrate, a thermal flux was used on this surface. To apply this thermal flux, the heat transfer coefficient (h) was assumed to be 25 $W/m^2.K$ [25].

As illustrated in Figure 5, in order to satisfy the mechanical boundary conditions, the point of the TBC system should be kept constant. In addition, the degree of freedom of the movement of all nodes located on the vertical surface of the TBC system should be closed in a horizontal direction to create symmetrical boundary conditions. On the contrary, the degree of freedom of their movement in the vertical direction should be kept

open.

Considering the dependence of the thermal and mechanical properties of the material on temperature, we gave the properties of different layers of TBC at different temperatures to the software as the inputs. Table 3 lists these thermal and mechanical properties of different layers of TBC [26-28]. In order to validate the proposed model in this study, a comparison was made between the simulation and experimental results obtained from the nanoindentation method.

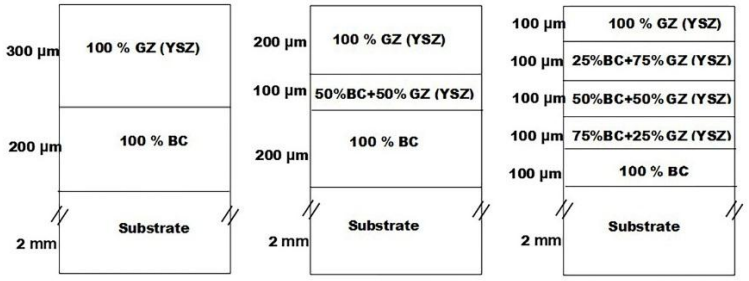

Figure 3. Schematic view of (a) duplex and functionally graded (b,c) coating designs

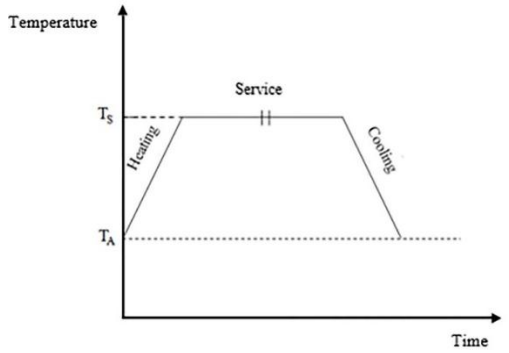

Figure 4. Thermal cycle applied at the highest level of thermal barrier coating

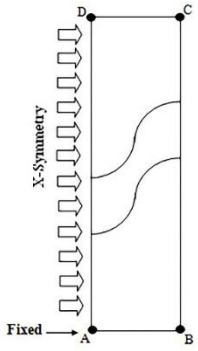

Figure 5. Assigning mechanical boundary conditions

TABLE 3. Thermal and mechanical properties of different layers of the thermal barrier coating [26–28]

Material properties	Temperature (K)	TGO Al_2O_3	Top Coat YSZ	Top Coat GZ	Bond Coat NiCrAlY	Substrate Hastelloy-X
E (GPa)	276	380	210	175	225	201
	673	338	205	170.8	186	180
	1073	-	181	150.8	147	150
	1473	312	162	135	134	141
P (Kg/m^3)	276 673 1073 1473	3978	5400	6320	7320	8220
υ	276 673 1073 1473	0.27	0.2	0.2	0.3	0.32
α ($\times 10^{-6}.K^{-1}$)	276	5.1	9.1	8.9	11.6	13.4
	673	-	10.58	9.04	14	14.2
	1073	-	11.13	10.08	16	15.6
	1473	9.8	8.5	10.9	20.8	15.8
C_p ($J.(kg.K)^{-1}$)	276	857	500	344	501	442
	673		576	430	592	514
	1073		637	456	781	668
	1473		650	460	764	831
K (W/m.°C)	276	25.2	1.06	1.11	4.3	10.4
	673		0.8	0.77	6.4	18.6
	1073		0.65	0.61	10.2	23.8
	1473		0.62	0.58	11.3	27.4

3. RESULTS AND DISCUSSION

Figure 6a shows the optical microscopy images of the structure of YSZ-based duplex TBC composed of three sections: substrate, bond coat, and top coat. The transparent areas represent the metal phases, dark gray areas the ceramic phases, and black areas the pores in the coating. The BC shown in a lighter color is a layered structure consisting of splats approximately parallel to the substrate surface. This microstructure is one of the main features of plasma spray coatings. As observed in Figure 6a,the interface between the layers of the TC and bond coats in the duplex TBC is clearly distinguished. Figure 6b shows the optical microscopy images of the structure of YSZ-based functionally graded TBC. According to this figure, the coating is characterized by a layered structure, and each layer contains micro cracks and pores that appear in black color. From the BC to the TC layer of the FG-TBC, the portion of NiCrAlY in the layers gradually changes. This gradient distribution of layers in the FG-TBC leads to the reduction of residual stresses caused by different CTEs between the metal and ceramic phases.

X-Ray Diffraction (XRD) analysis was carried out to distinguish between the phases of the initial (feedstock) powder and as-sprayed TC layer for Yttria stabilized Zirconia-based TBC, the results of which are shown in Figure 7. As observed in Figure 7a, the feedstock powder contains zirconium dioxide (ZrO_2) with the dominant structure of tetragonal phase in the form of partially stabilized zirconia and stabilized (non-transformable) zirconia and lower amount of cubic and monoclinic phases. As shown in Figure 7b, plasma spraying causes a significant reduction in the intensity of monoclinic phase. The as-sprayed coating is mostly composed of tetragonal phase with only traces of the monoclinic phase, and the amount of the cubic phase decreases in terms of the feedstock.

According to the equilibrium phase diagram of zirconia-yitria, the stable zirconia phase at room temperature contains 8 % of the weight of zirconia in the tetragonal phase. The non-transformable (stable) tetragonal phase is the main phase of plasma-sprayed zirconia which is formed as a result of rapid cooling of the whipped molten particles on the surface. In plasma spraying, a high proportion of Y_2O_3 (8 % by weight) in YSZ increases the phase temperature stability of the tetragonal ZrO_2 after cooling. Plasma spraying as a rapid process often leads to the formation of transformable (semi-stable) phases in the coating. In plasma sprayed TBCs, rapid cooling leads to the formation of a transformable (semi-stable) tetragonal phase (t') instead of a non-transformable (stable) tetragonal phase (t). In other words, rapid cooling during thermal spraying preserves the yttrium distribution of the primary powder in the tetragonal phase, thus leading to preservation of the transformable (semi-stable) tetragonal phase at room temperature. When the YSZ coating is semi-stable, and its chemical composition is the same as that of the more stable phase at higher temperatures, the chemical composition of the material will be mixed at room temperature rather than just the tetragonal phase predicted at room temperature. The resulting phases will be cubic and tetragonal [29,30].

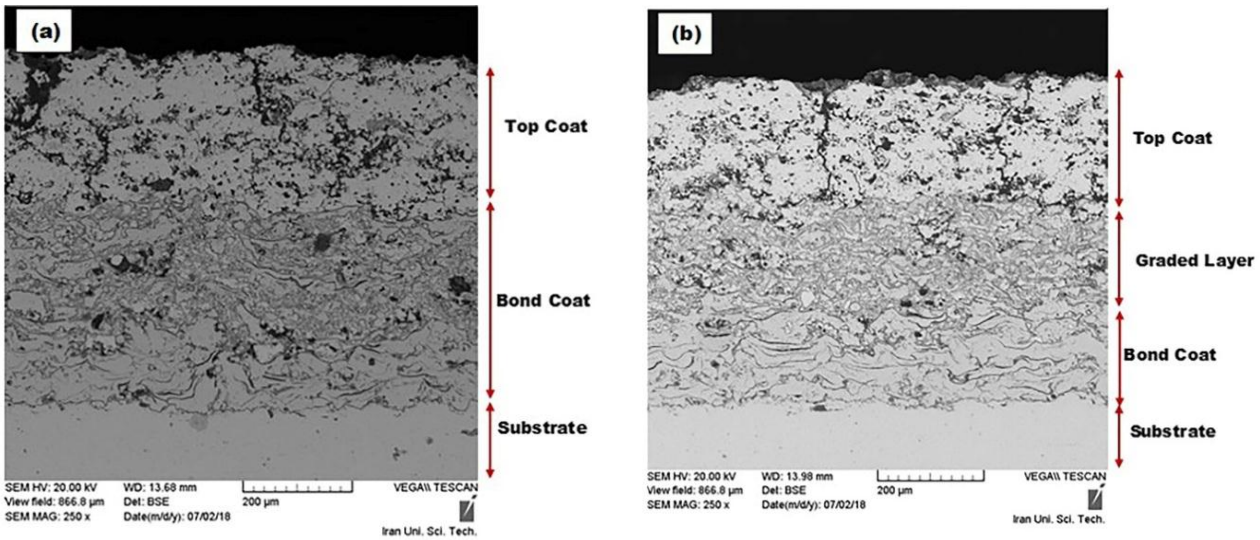

Figure 6. SEM images of the structure of (a) duplex coating and (b) functionally graded Yttria stabilized Zirconia based thermal barrier coating

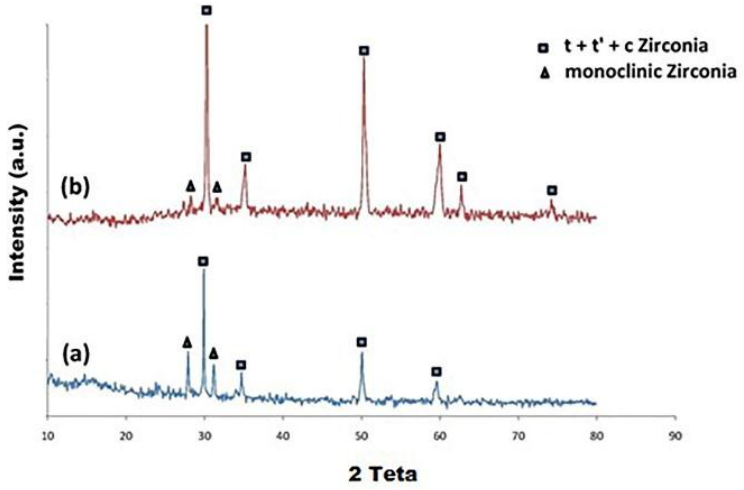

Figure 7. X-Ray Diffraction (XRD) analysis of a) the feedstock powder of YSZ-based top coat and b) as sprayed topcoat

Thermal spraying forms semi-stable compounds sensitive to the spray parameters. Even if the samples are coated with spray parameters that are as similar as possible (same source power, similar spray distance, etc.), the differences in the properties of the initial powder should be ignored. These changes in the properties of the initial powder result in different microstructures (porosity and pore properties) in the generated coatings. Therefore, the coatings differ in their properties, hence different phases of the sprayed coating [29,31,32].

High amount of cubic and monoclonal phases, instead of the tetragonal phase, is undesirable due to their lower mechanical properties. When cooled down to room temperature, the tetragonal phase is transformed into the monoclonal phase. This transformation is accompanied by an increase in the volume, hence creation of significant stress and possibly nucleation and crack growth within the TBC that would reduce the lifecycle of the coating [29–31].

As reported, the removal and depletion of yttrium (Y) from YSZ during operation and its exposure to high temperatures (above 1200 °C) and thermal cycling would form a monoclinic phase upon cooling to room temperature. As a result, the monoclinic phase is fromed based on the Y-depleted tetragonal phase during cooling. According to the findings, the higher the concentration of stabilizing elements in the tetragonal zirconia, the lower the proportion of formed monoclinic phase [29,32].

Normally, it is expected that no peak is found for monoclinic zirconia (m-ZrO_2) in the YSZ layer after spraying. However, in this study, XRD analysis confirmed the presence of small a amount of monoclinic phase in the TBC immediately after deposition (in the sprayed state), in addition to the presence of dominant non-transformable (stable) tetragonal (t-ZrO_2), convertible tetragonal (semi-stable) (t'-ZrO_2), and cubic phases. Apparantly, according to the spraying conditions in this study, all of the monoclinic phases in the YSZ powder cannot be removed. However, plasma spraying caused a significant reduction in the monoclonal phase in the primary powder.

Figure 8 depicts the SEM structure of duplex YSZ based-coating with map analysis of the elements. According to dot mapping of the elements, while Cr, Ni, and Al are mostly concentrated in the lower BC layer, Zr and Y are concentrated only in upper TC layer.

Figure 9 illustrates the SEM images of the structure of YSZ based-functionally graded coating as well as map analyses of elements. Dot mappings confirms that although Cr, Ni, and Al are mainly concentrated in lower BC layer, they are also present in the upper graded layers, hence a gradual change can be observed in Ni, Cr, and Al elements from the bond to top coats. In addition, a slight gradual distribution of Zr and Y from the top to the bond coats was observed. The results of SEM analysis revealed that microstructure, porosity, and chemical composition changed gradually through the functionally graded coating.

In order to carry out finite element analysis, a mesh sensitivity analysis was taken into account to determine the number of required elements in a model, thus ensuring that the analysis results were not affected by changing the mesh size The mesh sensivity is determined based on Figure 10 which shows the temperature change as a function of element size. Figure 11 shows the contour of the stress distribution S_{22} (in Pascal) for Gadolinium Zirconate-based TBC containing two-layer (duplex) thermal barrier, three-layer functionally graded thermal barrier, and five-layer functionally graded TBCs. According to Figure 11a, the maximum tensile stress and compressive stress in the duplex GZ-based TBC are about 19.42 MPa and 18.09 MPa, respectively. As observed in Figure 11b, the maximum tensile stress in the

GZ-based three-layer functionally graded TBC is reduced to 11.37 MPa. The gradual change in the thermal expansion coefficients of the FGM layers leads to better adhesion among the layers and lower stress concentration. As shown in Figure 11c, the maximum tensile stress in the GZ-based five-layer functionally graded TBC is 8.53 MPa, which is the least one compared to the maximum stress level in the two-layer thermal barrier and three-layer functionally graded TBCs. The simulation results of the stress distribution in the duplex and functionally graded GZ based TBC were in good agreement with those reported in the literature [18,29,30]. In the functionally graded TBC, the less difference between thermal expansions of layers would improve the adhesive bonding of ceramic/metal interface, thus avoiding later stress concentration and lessening the risk of crack initiation and propagation [11,33,34]. The maximum tensile stress in the three-layer functionally graded TBC was reduced by 41 %, compared to that of the two-layer TBC. In addition, the maximum tensile stress in the five-layer functionally graded TBC was reduced by 25 %, compared to that of the three-layer functionally graded TBC. This shows the effect of using functionally graded TBCs on both residual stress reduction and coating lifetime extension.

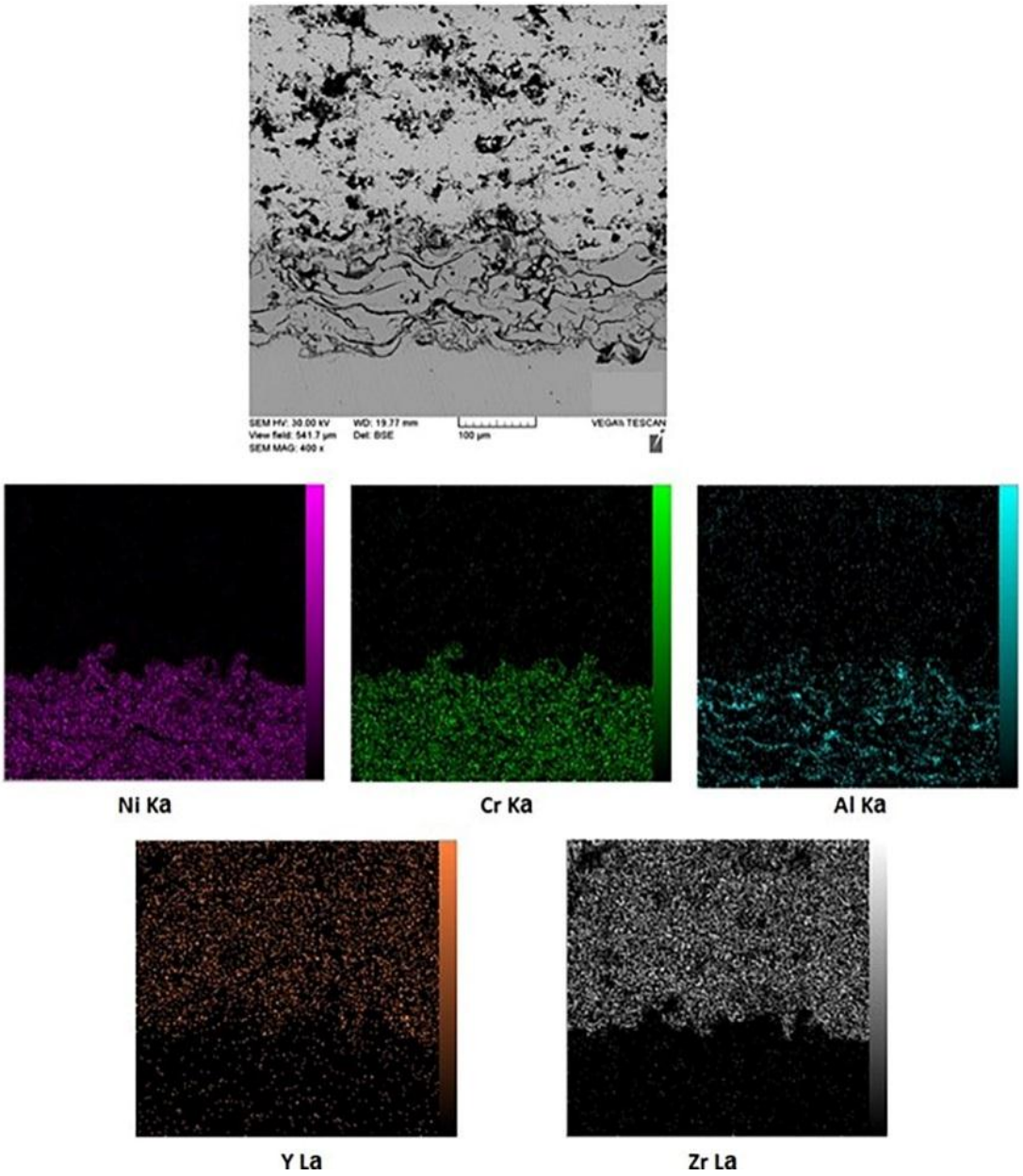

Figure 8. SEM image of the structure of YSZ/NiCrAlY coating with map analyses of elements

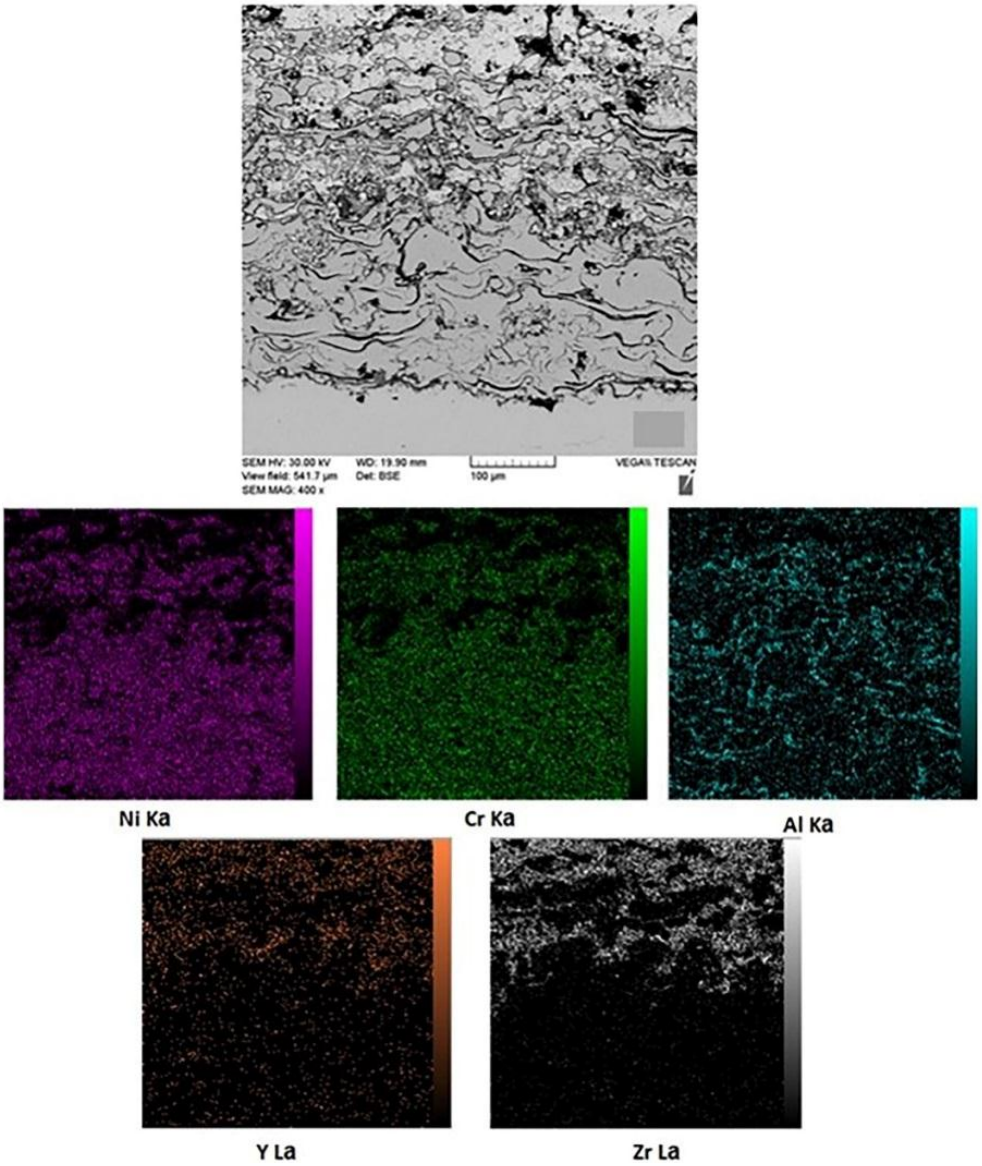

Figure 9. SEM image of the structure of Yttria stabilized Zirconia based functionally graded coating with map analyses of elements

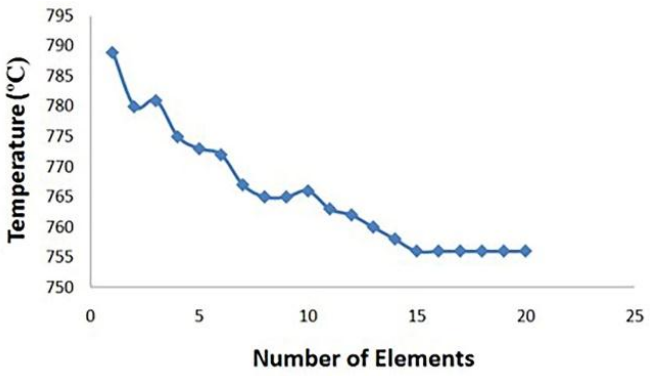

Figure 10. Mesh sensitivity analysis for TBC coating analysis

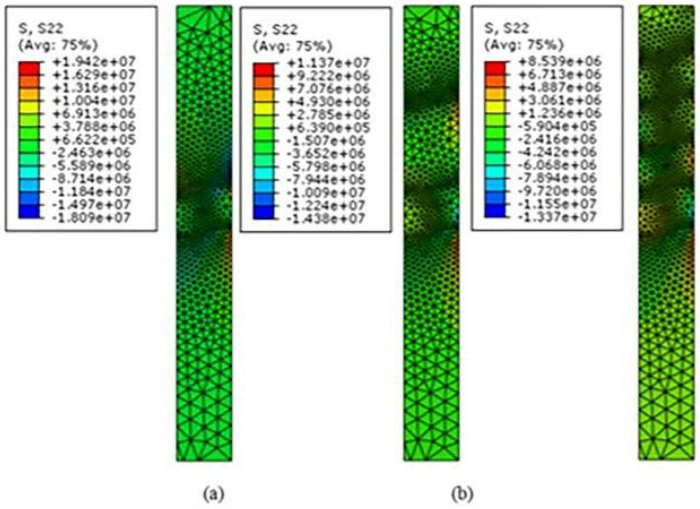

Figure 11. Stress distribution contours S22 (in Pascal) in Gadolinium Zirconate based thermal barrier coating a) duplex, b) three-layer FG-TBC, and c) five-layer FG-TBC

Figure 12 shows the contour of the stress distribution S22 (in Pascal) for Yttria stabilized Zirconia-based TBC: duplex (YSZ/NiCrAlY), a three-layer FG-TBC (YSZ/ 50 %YSZ + 50 %NiCrAlY/NiCrAlY) and a five-layer FG-TBC (YSZ/ 75 %YSZ + 25 %NiCrAlY/ 50 %YSZ + 50 %NiCrAlY/ 25 %YSZ + 75 %NiCrAlY/ NiCrAlY). Given that the thermal expansion of the BC is greater than that of the ceramic layer, compressive strength is observed in peak regions and tensile strength in valleys. In addition, a slow transition can be observed while approaching from the peak to the valley. The simulation results revealed that after the thermal shock, the average values of the maximum stress are 29 MPa for the duplex TBC (interface of TC / bond coat), 3.15 MPa for the three-layer FG-TBC system (interface of 50 % NiCrAlY - 50 %YSZ / YSZ), and 1.8 MPa for the five-layer FG-TBC system (interface of 25 % NiCrAlY- 75 % YSZ / YSZ). Of note, the stress distribution in the five-layer FG-TBC system is uniform which affects the performance and longevity of the thermal barrier system. The reason for this phenomenon is that the coefficient of the thermal expansion changed gradually throughout the five-layer functionally graded coating.

A comparison of Figures 11 and 12 confirms the higher amount of the residual stress in the Gadolinium zirconate-based TBC than that in the Yitria zirconate-based TBC. In Table 3, $\alpha_{GZ} < \alpha_{YSZ} < \alpha_{NiCrAlY}$; therefore, the difference in the thermal expansion coefficients of GZ and NiCrAlY is greater than that of YSZ and NiCrAlY, thus resulting in higher stress concentration.

As observed in Figure 13, the temperature distribution contours for the Gadolinium Zirconate-based TBC are shown in the following froms: two-layer (duplex) TBC, three-layer FG-TBC, and five-layer FG-TBC. The temperature difference between the TC surface and substrate in a three-layer TBC is 35 °C which is lower than that of two-layer (duplex) TBC, i.e., 62 °C. The three-layer functionally graded TBC has a 43 % lower insulating value than that of the two-layer TBC, and the five-layer functionally graded TBC has a 17 % lower insulating value than that of the three-layer functionally graded TBC mainly because the thickness of the TC of FG-TBCs is less than that of duplex TBCs. To provide thermal insulation, the layers near the surface (high temperature side) of FG-TBC should be ceramic rich. The composition gradually changes along the TBC thickness, from the ceramic-rich near the surface to the metal-rich near the coating-metallic substrate interface. The layers near the interface are metal-rich, thus having higher fracture toughness [33,34].

Figure 14 shows the temperature distribution contours of the two-layer, three-layer, and five-layer functionally graded Yttria stabilized Zirconia-based TBCs. The simulation results revealed that the temperature dropped by 102 °C along the duplex TBC. Thermal insulation was found to be reduced by 30 % in the functionally graded YSZ/NiCrAlY coatings, compared to duplex coatings. It was previously reported that the insulation value of FGTBCs was lower than that of conventional duplex YSZ TBCs with the same total coating thickness and YSZ porosity.The five-layer FG-TBC performs even worse than its three-layer counterpart due to a thinner YSZ top layer [35]. As observed in Figure 14, heat is primarily concentrated in the upper section of the coating system, and the substrate is protected from thermal damages. In other words, heat transfer is limited to the heat resistive ceramic parts while the BC and substrate experience lower temperatures, thus allowing for higher working temperatures. TBC protects the substrate from thermal load and keeps it at relatively lower

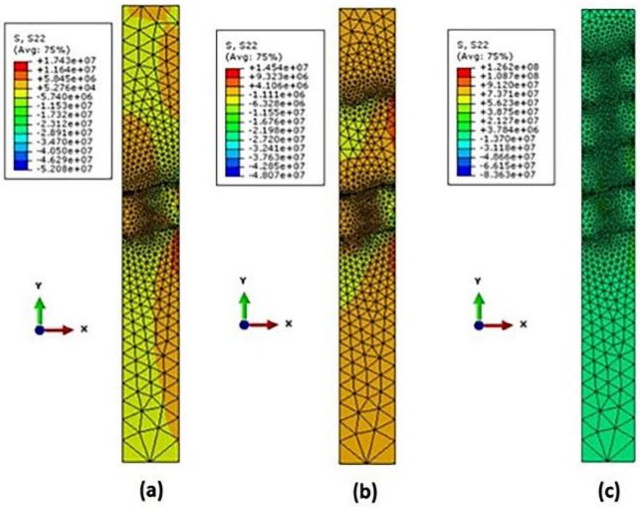

Figure 12. Stress distribution contours S_{22} (in Pascal) in Yittria Zirconate base thermal barrier coating a) duplex, b) three-layer FG-TBC, and c) five-layer FG-TBC

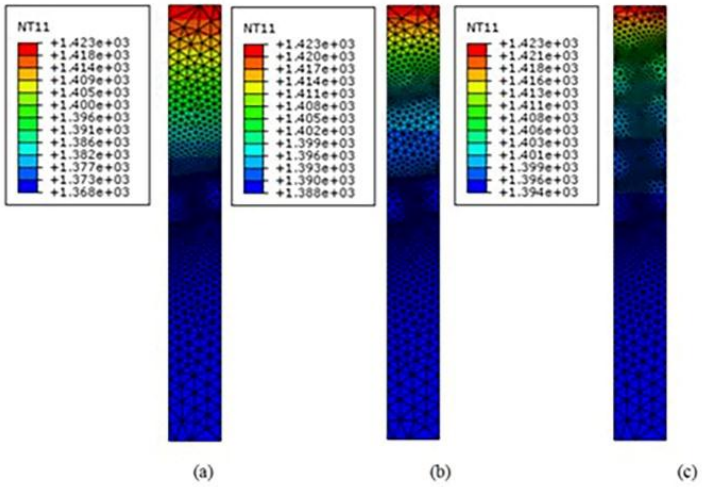

Figure 13. Temperature distribution contours in Gadolinium Zirconate based: a) two layer thermal barrier coating, b) three-layer functionally graded thermal barrier coating, and c) five-layer functionally graded thermal barrier coating

temperatures, thus resulting in an improved fatigue life, increased lifetime, and lower maintenance costs.

A comparison of Figures 13 and 14 revealed that the YSZ system exhibited better thermal insulation ability than GZ system. In addition, GZ had lower thermal conductivity (1.3 W/mK^{-1} at 1100 °C) than that of YSZ (1.8 W/mK^{-1} at 1100 °C). Consequently, it can be anticipated that GZ can provide better thermal insulation to the metallic substrate than YSZ. However, temperature reduction in the GZ system was even lower than that in the YSZ system. At 1500 °C, the YSZ system outperformed the GZ system approximately 39 %. According to the reports, the YSZ layer is characterized by more porosity than the GZ layer. YSZ also contains higher porosity content than that of GZ that can be justified by the lower melting temperature of GZ (2570 °C) than that of YSZ (2700 °C). Therefore, the GZ splats undergo a greater degree of melting temprature than that of YSZ, thus resulting in a relatively denser coating for GZ than that for YSZ. The dependence of the porosity of heat conductivity of coatings was taken into account to explain the lower thermal reduction of Gadolinium Zirconate-base TBC than that of the YSZ system [36,37].

Through an indentation fracture mechanics approach, the micro hardness, fracture toughness, and residual stress of the multiple-shocked TBC were evaluated. Figure 15 illustrates the load-displacement curve for the maximum force of 9000 μN.

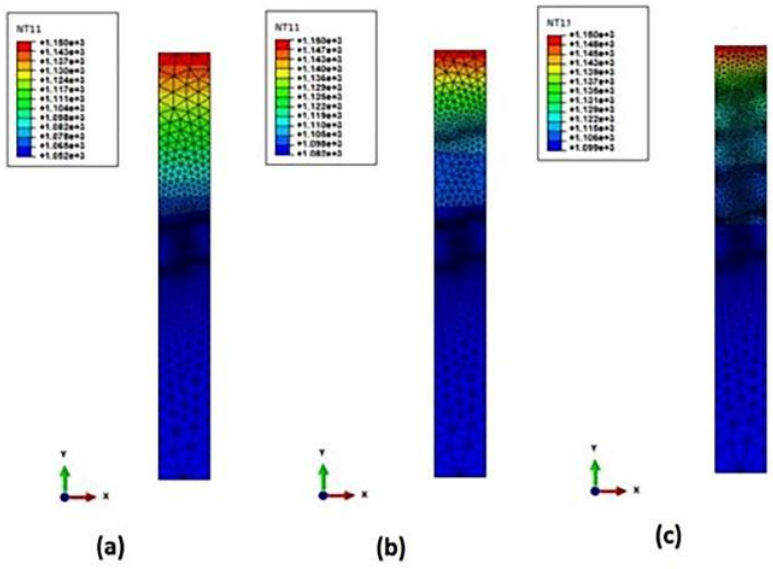

Figure 14. Temperature distribution contours in Yttria stabilized Zirconia based a) two layer thermal barrier coating, b) three-layer functionally graded thermal barrier coating, and c) five-layer functionally graded thermal barrier coating

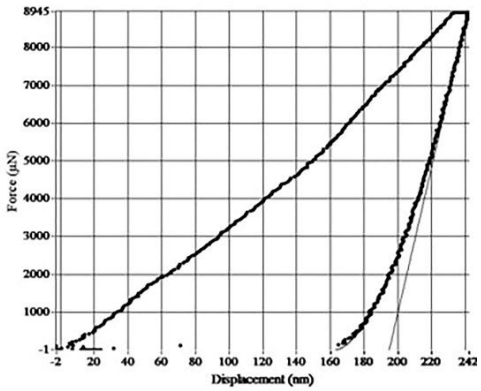

Figure 15. Load–displacement curve of the stressed three-layer YSZ-based FG-TBC under the maximum load of 9000 μN in the direction perpendicular to the cross-sectional area of the top coat

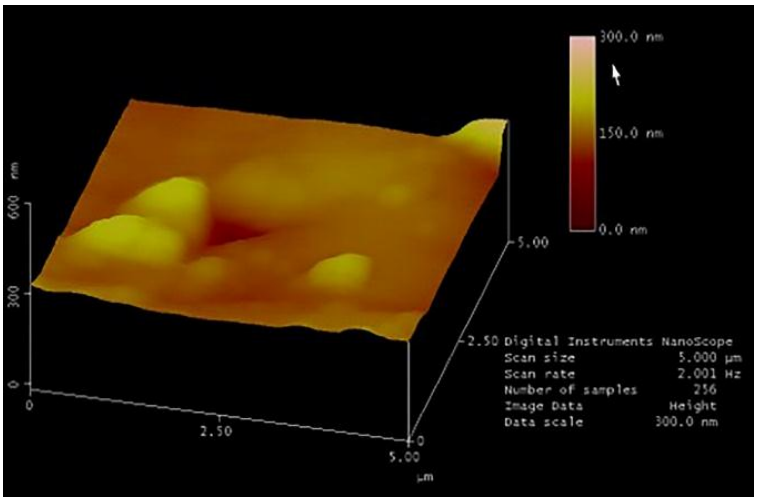

Figure 16. AFM images of impression by Berkovich indenter on the cross-section of the top coat layer of the stressed 3-layer YSZ-based FG-TBC under the maximum load of 8000 μN

Figure 16 depicts the AFM images of a Berkovich indenter impression on a stressed FG-TBC under the maximum load of 8000 N.

The relationship between the load and displacement from the initial unloading was used to calculate the Young's modulus, as shown in Equations (1)-(3). The values of the calculated hardness and Young's modulus in the TC are reported in Table 4. The size of the radial cracks was determined using image processing software. Two parameters P/C^2 and $C^{0.5}$ were then calculated using the mean length of radial cracks. The results are reported in Table 5 according to which, the diagram of $P/C^{1.5}$ was plotted in terms of $C^{0.5}$ (Figure 17). As mentioned earlier in Figure 17, $\left(-\frac{2\sigma}{\sqrt{\pi}\chi_i}\right)$ and $\left(\frac{K_{IC}}{\chi_i}\right)$ denote the slope and intercept of Equation (6), respectively. The calculation results of the Xi, K_{IC}, and residual stress are reported in Table 6, Table 7, and Table 8, respectively.

TABLE 4. Hardness and Young's modulus values for the top coat of stressed 3-layer YSZ- based FG-TBC

P	E_r	E_i	υ_i	Y	E	H
5000	178.6	1141	0.07	0.25	195.35	12.65
6000	185.8	1141	0.07	0.25	204.6	13.93
7000	211.6	1141	0.07	0.25	238.8	18.38
7500	190.5	1141	0.07	0.25	210.71	15.85
8000	111.5	1141	0.07	0.25	114.77	10.48
9000	211.7	1141	0.07	0.25	238.93	15.22

TABLE 5. The results of the calculation of the $P/C^{1.5}$ and $C^{0.5}$ and the mean length of the radial cracks

P(μN)	C_1(μm)	C_2(μm)	C_3(μm)	C_{avg}(μm)	C_{avg}(m)	$P/C^{1.5}(N/m^{1.5})*10^6$	$C^{0.5}(m^{0.5})$
5000	0.33	0.33	0.29	0.32	3.16E-07	28.15	0.00056
6000	0.38	0.38	0.42	0.39	3.93E-07	24.35	0.00063
7000	0.46	0.44	0.43	0.44	4.43E-07	23.74	0.00067
7500	0.54	0.53	0.55	0.54	5.40E-07	18.90	0.00073
8000	0.55	0.55	0.63	0.58	5.76E-07	18.30	0.00075
9000	0.54	0.58	0.62	0.58	5.80E-07	20.38	0.00076

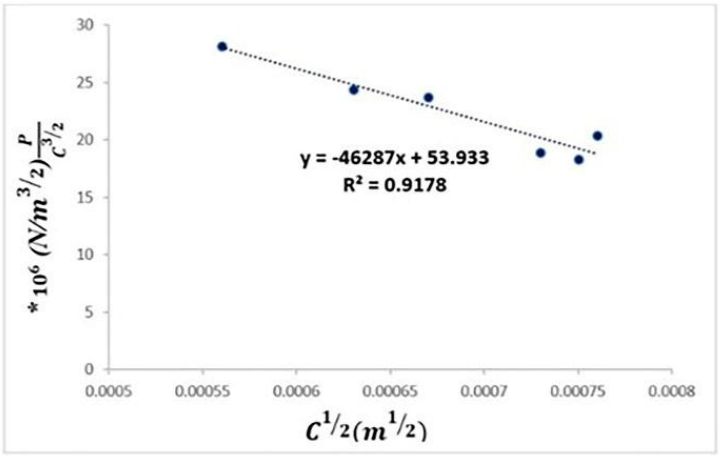

Figure 17. Relationships of $P/C^{1.5}$ versus $C^{0.5}$ when indented on the top coating surface

TABLE 6. Results of the calculation of the X_i

α	E_{avg}(GPa)	H_{avg}(GPa)	E/H	X_i
0.016	200.53	14.42	13.91	0.059

TABLE 7. Results of the calculation of the residual stress of stressed 3-layer YSZ- based FG-TBC

Slope	$\sigma\ (Pa)$	$\sigma\ (MPa)$
46287	100861-	0.100861-

TABLE 8. Results of the calculation of the fracture toughness of the stressed three-layer YSZ- based FG-TBC

α	E_{avg} (GPa)	H_{avg} (GPa)	E/H	X	Intercept	K_{IC} (MPa.m$^{1/2}$)
0.016	200.53	14.42	13.91	0.059	53.933	3.18

As validation or model evaluation, the stresses obtained from the nanoindentation method and simulation are presented in Table 9. The presented simulation is acceptable based on the low difference in the obtained results. The results from the stress measurement through nanoindentation method indicated that the designed method could measure the stress along the coating depth without damaging the sample.

TABLE 9. Comparison of the nanoindentation and simulation results of the stressed three-layer YSZ- based FG-TBC

Error percent	σ_{xx} (Simulation)	σ_{xx} (Nanoindentation)
2.84	-0.098 (MPa)	-0.100861 (MPa)

4. CONCLUSION

The current study aimed to investigate the thermal and residual stress distribution in the duplex and functionally graded Thermal Barrier Coatings (TBCs) of yttria-stabilized zirconia (YSZ) and gadolinium zirconate (GZ) during a realistic heating regime that includes heating, operating time, and final cooling. For this purpose, a finite element model was employed to model the effects of thermal loading on the thermomechanical response and stress distribution. In addition, three different YSZ-based TBC systems, one duplex, and two FG -TBCs, were fabricated using the APS method. The residual stress, elastic modulus, microhardness, and fracture toughness of the coating were determined using the nanoindentation stress measurement method. The FGM strategy reduced the stress values in the coating more significantly than the conventional coating. Small differences in the thermal expansion would improve the adhesive bond between different ceramic/metal interfaces and reduce the risk of crack initiation and propagation. According to the findings, the level of residual stress in the functionally graded TBC was lower than that in the duplex TBC, and the stress distribution was more uniform, hence performance improvement and longevity expansion of the thermal barrier system. The results also indicated that most of the damage and heat fluxes were concentrated and accumulates in the ceramic face layers, hence less damage and shortened substrate life. Examination of the surface of the specimens after the application of thermal shock revealed that the separation of the layers occurred more frequently in the two-layer TBCs than in the graded coatings. The results of stress measurement through the nanoindentation method showed that the developed stress measurement method could measure stress along the coating depth without damaging the specimen. It was also found that the TBC based on yttria-stabilized zirconia was slightly better than the that based on GZ in terms of thermal shock resistance and residual stress.

ACKNOWLEDGEMENTS

The authors would like to appreciate Iran University of Science and Technology and Standard Research Institute for their support.

REFERENCES

1. Liu, B., Liu, Y., Zhu, C., Xiang, H., Chen, H., Sun, L., Gao, Y., Zhou, Y., "Advances on strategies for searching for next generation thermal barrier coating materials", ***Journal of Materials Science & Technology***, Vol. 35, No. 5, (2019), 833-851. https://doi.org/10.1016/j.jmst.2018.11.016
2. Fathi Dehkharghani, A. M., Rahimipour, M. R., Zakeri. M., "Crystal Structure and Lattice Parameter Investigation of La_3+ Substituted CeO_2 in $La_xCe_{1-x}O_{2-X/2}$ Synthesized by Solid-State Method", ***Advanced Ceramics Progress***, Vol. 6, No. 1, (2020), 43-48. https://doi.org/10.30501/acp.2020.106445
3. Clarke, D. R., Phillpot. S. R., "Thermal Barrier Coating Materials", ***Materials Today***, Vol. 8, No. 6, (2005), 22–29. https://doi.org/10.1016/S1369-7021(05)70934-2
4. Dean, J., Aldrich-Smith, G., Clyne. T. W., "Use of Nanoindentation to Measure Residual Stresses in Surface Layers", ***Acta Materialia***, Vol. 59, No. 7, (2011), 2749-2761. https://doi.org/10.1016/j.actamat.2011.01.014
5. Doleker, K. M., Ozgurluk, Y., Ahlatci, H., Karaoglanli, A. C., "Evaluation of Oxidation and Thermal Cyclic Behavior of YSZ, $Gd_2Zr_2O_7$ and YSZ/$Gd_2Zr_2O_7$ TBCs", ***Surface and Coatings Technology***, Vol. 371, (2019), 262-275. https://doi.org/10.1016/j.surfcoat.2018.11.055
6. Ge, W. A., Zhao, C. Y., Wang. B. X., "Thermal radiation and conduction in functionally graded thermal barrier coatings. part I: experimental study on radiative properties", ***International Journal of Heat and Mass Transfer***, Vol. 134, (2019), 101–13. https://doi.org/10.1016/j.ijheatmasstransfer.2019.01.018
7. Goswami, B., Ray, A. K., Sahay. S. K. "Thermal barrier coating system for gas turbine application-a review", ***High Temperature Materials and Processes***, Vol. 23, No. 2, (2004), 73–92. https://doi.org/10.1515/HTMP.2004.23.2.73
8. Karaoglanli, A. C., Altuncu, E., Ozdemir, I., Turk, A., Ustel, F., "Structure and durability evaluation of YSZ+Al_2O_3 composite TBCs with APS and HVOF bond coats under thermal cycling conditions", ***Surface and Coatings Technology***, Vol. 205, (2011), S369-S373. https://doi.org/10.1016/j.surfcoat.2011.04.081

9. Kese, K., Rowcliffe, D. J., "Nanoindentation method for measuring residual stress in brittle materials", ***Journal of the American Ceramic Society***, Vol. 86, No. 5, (2003), 811-816. https://doi.org/10.1111/j.1151-2916.2003.tb03380.x
10. Khoddami, A. M., Sabour, A., Hadavi, S. M. M., "Microstructure formation in thermally-sprayed duplex and functionally graded NiCrAlY/Yttria-Stabilized zirconia coatings", ***Surface and Coatings Technology***, Vol. 201, No. 12, (2007), 6019-6024. https://doi.org/10.1016/j.surfcoat.2006.11.020
11. Kokini, K., DeJonge, J., Rangaraj, S., Beardsley, B., "Thermal shock of functionally graded thermal barrier coatings with similar thermal resistance", ***Surface and Coatings Technology***, Vol. 154, No. 2-3, (2002), 223-231. https://doi.org/10.1016/S0257-8972(02)00031-2
12. Liu, B., Liu, Y., Zhu, C., Xiang, H., Chen, H., Sun, L., Gao, Y., Zhou, Y., "Advances on strategies for searching for next generation thermal barrier coating materials", ***Journal of Materials Science & Technology***, Vol. 35, No. 5, (2019), 833-851. https://doi.org/10.1016/j.jmst.2018.11.016
13. Liu, Z. G., Ouyang, J. H., Zhou, Y., "Heat capacities and derived thermodynamic functions of neodymium-cadolinium zirconates from 298.15 to 1050 K", ***Journal of Alloys and Compounds***, Vol. 475, No. 1-2, (2009), 21-24. https://doi.org/10.1016/j.jallcom.2008.07.089
14. Mahade, S., Curry, N., Björklund, S., Markocsan, N., Joshi, S., "Durability of gadolinium zirconate/YSZ double-layered thermal barrier coatings under different thermal cyclic test conditions", ***Materials***, Vol. 12, No. 14, (2019), 2238. https://doi.org/10.3390/ma12142238
15. Nayebpashaee, N., Seyedein, S. H., Aboutalebi, M. R., Sarpoolaky, H., Hadavi, M. M., "Modeling the effect of interface characteristics and layer compositional parameters on the residual stress distribution in FG-TBC system: FEM and FIS approach", ***Journal of Ceramic Processing Research***, Vol. 17, No. 8, (2016), 803-814. http://www.jcpr.or.kr/journal/archive/view/1933#
16. Nayebpashaee, N., Seyedein, S. H., Aboutalebi, M. R., Sarpoolaky, H., Hadavi, S. M. M., "Finite element simulation of residual stress and failure mechanism in plasma sprayed thermal barrier coatings using actual microstructure as the representative volume", ***Surface and Coatings Technology***, Vol. 291 (2016), 103-114. https://doi.org/10.1016/j.surfcoat.2016.02.028
17. Nayebpashaee, N., Aboutalebi, M. R., Seyedein, S. H., Sarpoolaky, H., Hadavi, M. M., "Simulation of the effect of sub-micron interface roughness on the stress distribution in functionally graded thermal barrier coatings (FG-TBC)", ***Advanced Ceramics Progress***, Vol. 1, No. 1, (2015), 40-47. https://doi.org/10.30501/acp.2015.69999
18. NayebPashaee, N., Vafaeenezhad, H., Hadavi, S. M. M., Seyedein, S. H., Aboutalebi, M. R., Sarpoolaky, H. "A study on the numerical simulation of thermo-mechanical behavior of the novel functionally graded thermal barrier coating under thermal shock", ***ADMT Journal***, Vol. 8, No. 2, (2015), 29-36. http://admt.iaumajlesi.ac.ir/article_534924_6096e9df4f341acab0b97c321312d785.pdf
19. Oliker, V. E., Gridasova, T. Y., Pritulyak, A. A., "Effect of the porous structure of thermal-barrier coatings on their heat conductivity", ***Powder Metallurgy and Metal Ceramics***, Vol. 47, No. 11, (2008), 717-722. https://doi.org/10.1007/s11106-009-9066-2
20. Ranjbar-Far, M., Absi, J., Mariaux. G., "Finite element modeling of the different failure mechanisms of a plasma sprayed thermal barrier coatings system", ***Journal of Thermal Spray Technology***, Vol. 21, No. 6, (2012), 1234-1244. https://doi.org/10.1007/s11666-012-9814-6
21. Ranjbar-Far, M., Absi, J., Shahidi, S., Mariaux, G., "Impact of the non-homogenous temperature distribution and the coatings process modeling on the thermal barrier coatings system", ***Materials & Design***, Vol. 32, No. 2, (2011), 728-735. https://doi.org/10.1016/j.matdes.2010.07.034
22. Song, J., Qi, H., Shi, D., Yang, X., Li, S., "Effect of non-uniform growth of TGO layer on cracking behaviors in thermal barrier coatings: A numerical study", ***Surface and Coatings Technology***, Vol. 370, (2019), 113-124. https://doi.org/10.1016/j.surfcoat.2019.04.069
23. Mao, W. G., Wan, J., Dai, C. Y., Ding, J., Zhang, Y., Zhou, Y. C., Lu, C., "Evaluation of microhardness, fracture toughness and residual stress in a thermal barrier coating system: A modified vickers indentation technique", ***Surface and Coatings Technology***, Vol. 206, No. 21, (2012), 4455-4461. https://doi.org/10.1016/j.surfcoat.2012.02.060
24. Thakare, J. G., Pandey, C., Mahapatra, M. M., Mulik, R. S., "Thermal barrier coatings—a state of the art review", ***Metals and Materials International***, Vol. 27, No. 7, (2021), 1947-1968. https://doi.org/10.1007/s12540-020-00705-w
25. Vaßen, R., Jarligo, M. O., Steinke, T., Mack, D. E., Stöver, D., "Overview on advanced thermal barrier coatings", ***Surface and Coatings Technology***, Vol. 205, No. 4, (2010), 938-942. https://doi.org/10.1016/j.surfcoat.2010.08.151
26. Yang, F., Li, J. C. M., ***Micro and Nano Mechanical Testing of Materials and Devices***, New York: Springer, (2008). https://doi.org/10.1007/978-0-387-78701-5
27. Johari, A. D., Yunus, S. M., Husin, S., "Comparison on thermal resistance performance of YSZ and rare-earth GZ multilayer thermal barrier coating at 1250°C gas turbine combustor liner", ***Journal of Advanced Research in Fluid Mechanics and Thermal Sciences***, Vol. 52, No. 2, (2018), 123-128. https://www.akademiabaru.com/submit/index.php/arfmts/article/download/2383/1344
28. Zhang, P., Feng, Y., Li, Y., Pan, W., Zong, P. A., Huang, M., Han, Y., Yang, Z., Chen, H., Gong, Q., Wan, C., "Thermal and mechanical properties of ferroelastic $RENbO_4$ (RE = Nd, Sm, Gd, Dy, Er, Yb) for thermal barrier coatings", ***Scripta Materialia***, Vol. 180 (2020), 51–56. https://doi.org/10.1016/j.scriptamat.2020.01.026
29. Lima, R. S., Marple, B. R., "Thermal spray coatings engineered from nanostructured ceramic agglomerated powders for structural, thermal barrier and biomedical applications: a review", ***Journal of Thermal Spray Technology***, Vol. 16, No. 1, (2007), 40-63. https://doi.org/10.1007/s11666-006-9010-7
30. Ilavsky, J., Stalick, J. K., "Phase composition and its changes during annealing of plasma-sprayed YSZ", ***Surface and Coatings Technology***, Vol. 127, No. 2-3 (2000), 120-129. https://doi.org/10.1016/S0257-8972(00)00562-4
31. Di Girolamo, G., Blasi, C., Pagnotta, L., Schioppa, M., "Phase evolution and thermophysical properties of plasma sprayed thick zirconia coatings after annealing", ***Ceramics International***, Vol. 36, No. 8, (2010), 2273-2280. https://doi.org/10.1016/j.ceramint.2010.07.035
32. Osorio, J. D., Lopera-Valle, A., Toro, A., Hernández-Ortiz, J. P., "Phase transformations in air plasma-sprayed yttria-stabilized zirconia thermal barrier coatings", ***Dyna***, Vol. 81, No. 185, (2014), 13-18. https://doi.org/10.15446/dyna.v81n185.33409
33. Zhao, X., Xiao. P., "Residual stresses in thermal barrier coatings measured by photoluminescence piezospectroscopy and indentation technique", ***Surface and Coatings Technology***, Vol. 201, No. 3-4, (2006), 1124-1131. https://doi.org/10.1016/j.surfcoat.2006.01.035
34. Zhu, J., Xie, H., Hu, Z., Chen, P., Zhang, Q., "Cross-sectional residual stresses in thermal spray coatings measured by moiré interferometry and nanoindentation technique", ***Journal of Thermal Spray Technology***, Vol. 21, No. 5, (2012), 810-817. https://doi.org/10.1007/s11666-012-9732-7
35. Zhu, L. N., Xu, B. S., Wang, H. D., Wang, C. B., "Measurement of residual stresses using nanoindentation method", ***Critical Reviews in Solid State and Materials Sciences***, Vol. 40, No. 2 (2015), 77-89. https://doi.org/10.1080/10408436.2014.940442

36. Mahade, S., Curry, N., Björklund, S., Markocsan, N., Joshi, S., "Durability of gadolinium zirconate/YSZ double-layered thermal barrier coatings under different thermal cyclic test conditions", ***Materials***, Vol. 12, No. 14, (2019), 2238. https://doi.org/10.3390/ma12142238

37. Mahade, S., Curry, N., Jonnalagadda, K. P., Peng, R. L., Markocsan, N., Nylén, P., "Influence of YSZ layer thickness on the durability of gadolinium zirconate/YSZ double-layered thermal barrier coatings produced by suspension plasma spray", ***Surface and Coatings Technology***, Vol. 357, (2019), 456-465. https://doi.org/10.1016/j.surfcoat.2018.10.046